Available online at www.sciencedirect.com
ScienceDirect
Journal of Asian Earth Sciences 32 (2008) 385–395
Journal of Asian Earth Sciences
www.elsevier.com/locate/jaes

Geology and geochemistry of the Shuanggou ophiolite (Ailao Shan ophiolitic belt), Yunnan Province, SW China: Evidence for a slow-spreading oceanic basin origin

Graciano P. Yumul Jr. [a,d,*], Mei-Fu Zhou [b], Christina Yan Wang [b], Tai-Ping Zhao [c], Carla B. Dimalanta [a]

[a] National Institute of Geological Sciences, College of Science, University of the Philippines, Diliman, Philippines
[b] Department of Earth Sciences, The University of Hong Kong, Hong Kong, China
[c] Guangzhou Institute of Geochemistry, Chinese Academy of Sciences, Guangzhou, China
[d] The Philippine Council for Industry and Energy Research and Development, Department of Science and Technology, Metro Manila, Philippines

Abstract

The early Carboniferous Shuanggou ophiolite lies in the middle segment of the Ailao Shan orogenic belt between the South China Block to the north and the Indochina Block to the south. The ophiolite consists of meta-peridotite, gabbro, diabase and basalt, capped by radiolarian-bearing siliceous rocks. No layered gabbros or sheeted dikes have been observed. The meta-peridotite underwent low degrees of partial melting, consistent with the low magma budget of this oceanic lithosphere. Whole-rock rare earth element analyses of gabbro indicate a geochemical affinity with normal mid-ocean ridge basalts, consistent with the crystallization order of plagioclase followed by clinopyroxene recognized in the gabbros. The ophiolite is believed to have formed in a small, slow-spreading oceanic basin. Collision of the Indochina Block with the South China Block in the late Paleozoic was responsible for the closure of the oceanic basin and emplacement of the ophiolite in the Ailao Shan orogenic belt.

Keywords: Slow-spreading basin; Ophiolite; Geochemistry; Shuanggou; Ailao Shan; China

1. Introduction

The South China and Indochina Blocks were once separated by eastern Paleo-Tethys. The amalgamation of these two blocks is now clearly marked by the 900 km long Ailao Shan suture zone, extending from SW China to northern Vietnam (Fig. 1), although the zone has been extensively modified by Tertiary left-lateral strike-slip movement on the Ailao Shan–Red River Fault (RRF) (Tapponnier et al., 1990; Leloup et al., 1993, 2001). Numerous ophiolites occur in the suture zone and these may shed light on the origin and evolution of eastern Paleo-Tethys (Metcalfe, 1996; Chen and Xie, 1994). However, the original tectonic environment in which the ophiolites formed has long been controversial and remains uncertain. For example, the ophiolites have variously been interpreted to have formed in a wide ocean (Mo et al., 1993), a back-arc basin (Pan et al., 1997; Hsu et al., 1995), a remnant oceanic basin (Li et al., 1991), or a small oceanic basin (Sun et al., 1997). The ages of the origin, spreading and subduction of this ocean basin are not yet fully constrained.

In this paper, we integrate the available geological information on the ophiolites along the RRF and present new petrographic and geochemical data for the Shuanggou ophiolite, the best-preserved body in the Ailao Shan suture zone. Available field evidence and geochemical data suggest formation in a slow-spreading oceanic basin. Using

* Corresponding author. Address: National Institute of Geological Sciences, College of Science, University of the Philippines, Diliman, Philippines. Tel.: +63 2 9296047; fax: +63 2 4395924/8372925.
E-mail addresses: rwg@i-next.net, rwgmails@yahoo.com, csrwg@yahoo.com (G.P. Yumul Jr.).

1367-9120/$ - see front matter © 2007 Elsevier Ltd. All rights reserved.
doi:10.1016/j.jseaes.2007.11.007

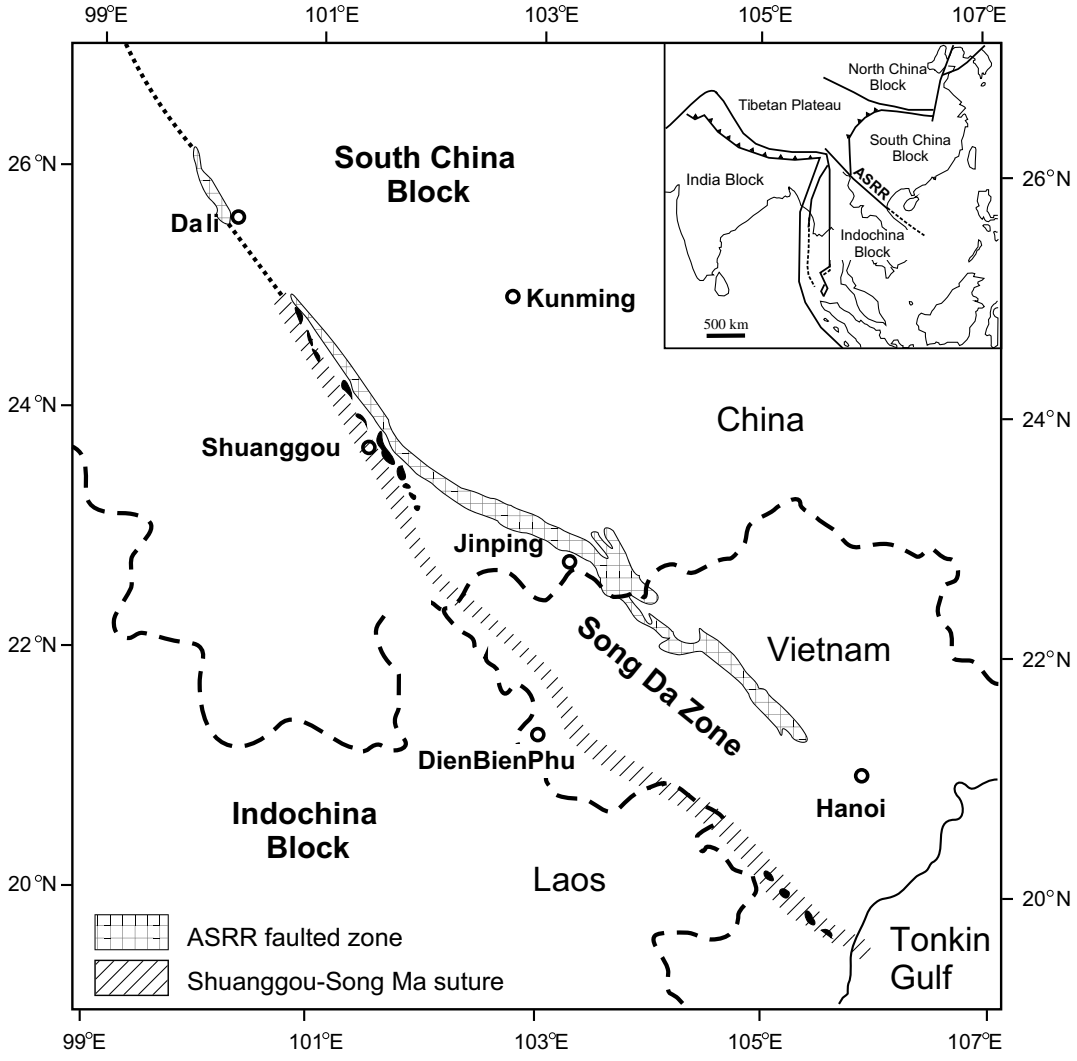

Fig. 1. Regional map of southwest China and northern Vietnam showing the location of the Song Da zone and the Ailao Shan orogenic belt. Inset shows the position of the suture zone in Yunnan Province and location of the Shuanggou ophiolite. ASRR = Ailao Shan Red River.

these data, we present a model for the tectonic evolution of the ophiolite belt.

2. Regional geological background

The Ailao Shan orogenic belt extends for over 900 km from the Day Nui Con Voi range in northern Vietnam to the Ailao Shan, Diancang Shan and Xuelong Shan in Yunnan, SW China (Fig. 2). It separates the South China Block on the northeast from the Indochina Block on the southwest. The 10 km wide zone contains hundreds of ophiolitic mafic–ultramafic bodies that lie between high-grade gneiss on the east and an island arc volcano-sedimentary belt on the west. The ophiolite zone is bounded by the Ailao Shan fault on the east and the Amojiang fault on the west (Yunnan, 1990; Dong et al., 2000). The mafic–ultramafic bodies have been thrust westward over the Phanerozoic Ailao Shan metamorphic belt.

The ultramafic rock bodies are typically a few tens to hundreds of meters long with length/width ratios of about 3:1–40:1. A few are over 1000 m long and the largest is about 15 km long and 2 km wide. Mafic rock bodies are typically hundreds of meters long with length/width ratios of about 2:1–15:1 with the largest being about 11–14 km long and 300–1000 m wide. Individual rock bodies are elongate parallel to the regional tectonic orientation and crop out as tectonic slices (Yunnan, 1990).

In northern Vietnam, about 120 km south of the Red River, ultramafic rocks are exposed over a distance of about 170 km along the NW–SE-striking Song Ma suture zone (e.g., Hutchinson, 1975, 1989; Sengor, 1984, 1987). These ultramafic rocks are in fault contact with early Paleozoic to Permian sedimentary strata associated with late Permian to early Triassic siliceous shale and basaltic lava (Pan et al., 1997). These rocks, which appear to have been thrust northward, crop out along a belt of reportedly Paleozoic metamorphic rocks. South of this belt, Siluro-Devonian shale and silicic tuff are intruded by granodiorite and granite.

The Shuanggou ophiolite extends for about 8 km in a NNW direction and is up to 2.5 km wide. It is the best-pre-

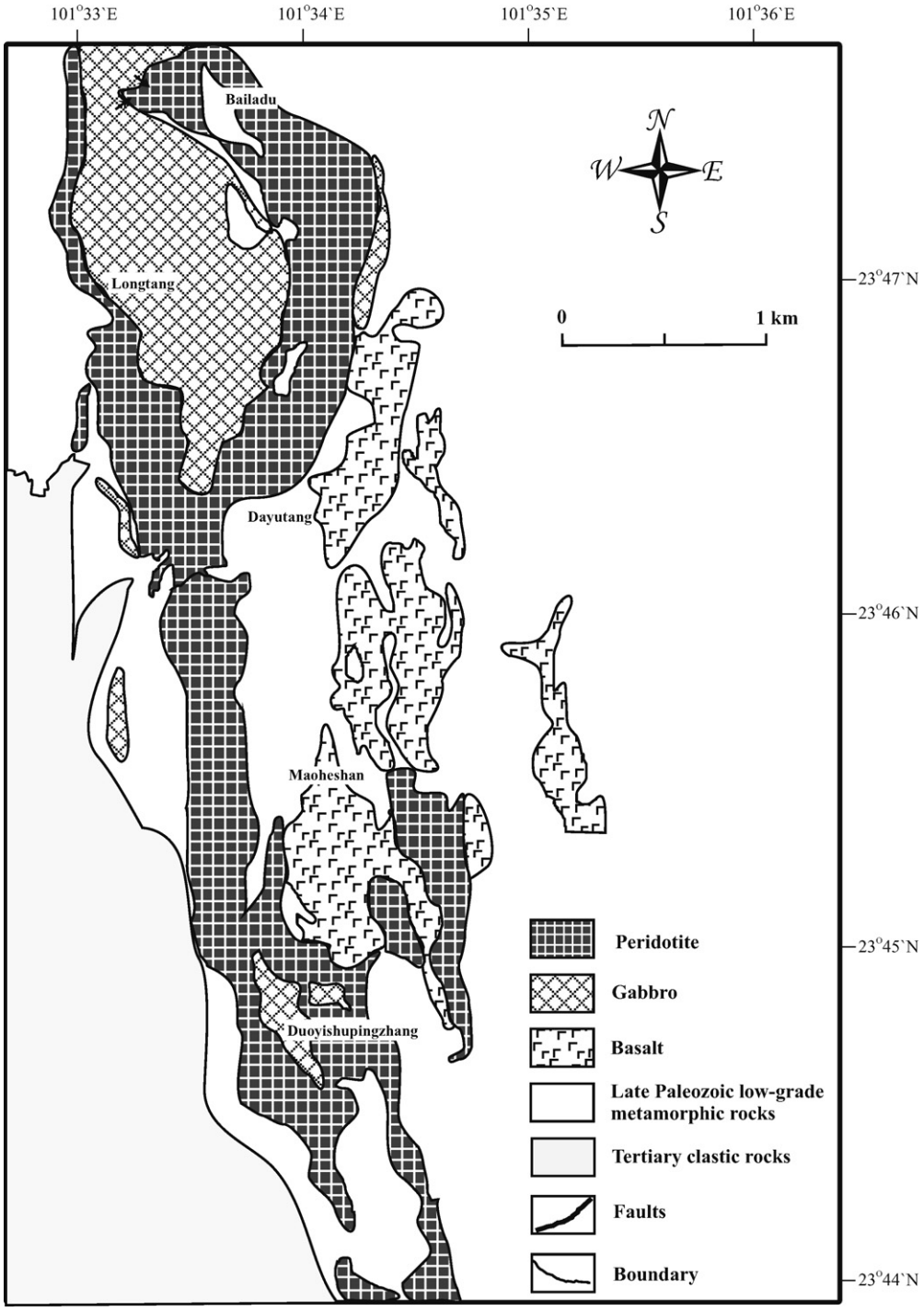

Fig. 2. Geologic map of the Shuanggou ophiolite.

served and best-studied body in the belt, and is considered to be representative of the Ailao Shan ophiolites (Fig. 2).

3. Geology and petrography of the Shuanggou ophiolite

The Shuanggou ophiolite is composed of three main units from the base upward: meta-peridotite, diabase–gabbro and basalt (Fig. 2). No layered gabbro or sheeted dikes have been recognized. The meta-peridotite, at the base of the section, is overlain tectonically by a crustal assemblage composed of diabase, gabbro and pegmatitic gabbro. Some of the gabbros contain diabase xenoliths and have been intruded by pegmatitic zones. The basalt is in fault contact with the meta-peridotite, but the relationship between the basalt and the diabase–gabbro assemblage is not clear.

Although strongly serpentinized, the meta-peridotite is identified as mostly lherzolite with minor harzburgite. Both the lherzolite and harzburgite consist of olivine,

orthopyroxene, clinopyroxene and spinel (some contain grossular instead), and they differ chiefly in their modal percent of clinopyroxene. Both have minor impregnations of clinopyroxene and plagioclase. They mostly have protogranular and porphyroblastic textures (terminology following Mercier and Nicolas, 1975), with a schistose matrix. Kink banding and undulatory extinction are common in the olivine and pyroxene grains. The olivine is altered to serpentine, chlorite and magnetite whereas orthopyroxene is altered to bastite. Spinel grains are reddish-brown and range in shape from amoeboid to euhedral. Plagioclase blebs, altered to clay, were noted in some samples.

The gabbros have subhedral granular textures, and are composed of uralitized pyroxene and saussuritized plagioclase with minor veins of zoisite and amphibole. Most are adcumulates although mesocumulate and orthocumulate varieties are also present. In the adcumulate rocks, large euhedral crystals of plagioclase and clinopyroxene are the cumulus minerals. Most of the clinopyroxene crystals contain small inclusions of plagioclase, and exsolution lamellae of orthopyroxene are present in some grains. Bent lamellae and undulatory extinction in the clinopyroxene and, to a lesser extent, plagioclase crystals suggest some deformation. Post-cumulus minerals are chiefly small, anhedral clinopyroxene grains. The dominant crystallization order for the gabbro is plagioclase → clinopyroxene → magnetite. Locally, the gabbro grades into diorite composed of primary hornblende and sericitized plagioclase with minor quartz. Plagioclase in the gabbros is variably altered to clay and chlorite whereas clinopyroxene is altered to chlorite and uralite.

The diabases have ophitic textures, and consist of plagioclase, pyroxene, hornblende and ilmenite. Sparse plagioclase phenocrysts are altered to clay and calcite. Clinopyroxene is altered to chlorite.

The mafic lavas are fine-grained, sparsely phyric rocks with intersertal textures. Most of the rocks are highly altered and the degree of alteration generally increases upward (Wei et al., 1999). Secondary minerals include albite, chlorite and minor epidote.

4. Analytical methods

Samples were cut with a diamond-impregnated brass blade, crushed in a steel jaw crusher that was brushed and cleaned with de-ionized water between samples, and pulverized in an agate mortar in order to minimize potential contamination. Major oxides were determined by wavelength-dispersive X-ray fluorescence spectrometry (WD-XRFS) of fused glass beads using a Philips PW2400 spectrometer at the University of Hong Kong. Selected trace elements, including Sc, V, Cr, Ni, Zn and Cu, were analyzed by WD-XRFS on pressed powder pellets. Additional trace elements, including the REE, were determined by inductively-coupled plasma mass spectrometry (ICP-MS) of nebulized solutions using a VG Plasma-Quad Excell ICP-MS, also at the University of Hong Kong. The solutions were produced by a 2-day closed beaker digestion using a mixture of HF and HNO_3 acids in high-pressure bombs (Qi et al., 2000). Pure elemental standard solutions were used for external calibration and BHVO-1 and SY-4 were used as reference materials. The accuracies of the XRF analyses are estimated to be ±1% (relative) for SiO_2, ±2% for the other major oxides present in concentrations greater than 0.5 wt% and ±5% (relative) for minor oxides present in concentrations greater than 0.1%. The accuracies of the ICP-MS analyses are estimated to be better than ±5% (relative) for most elements.

5. Analytical results

Analytical results for 7 meta-peridotite, 3 diabase and 15 gabbro samples are listed in Table 1. The major oxide data presented in Table 1 are measured values but the values in Figs. 2–4, as well as those in the following discussion, have been normalized to 100% on an anhydrous basis.

5.1. Meta-peridotite

The meta-peridotites have all been extensively serpentinized as indicated by their high loss on ignition (LOI). However, despite the high degree of alteration, the major element concentrations do not appear to have been greatly modified. For example, the Mg#s [$100Mg/(Mg + Fe^{2+})$] of the meta-peridotites range from 87 to 91 (average 89). In addition, the major oxide contents are compatible with the mineralogical compositions. As expected, the harzburgites have the highest MgO contents (average 42.4 wt%) (Mg# = 91), but relatively low CaO (average 0.5 wt%), Al_2O_3 (average 2.4 wt%) and TiO_2 (average 0.05 wt%), and are similar to highly depleted harzburgites, such as those in the Troodos ophiolite of Cyprus. The lherzolite has slightly lower MgO (40.9 wt%) and Mg# (90) and relatively high CaO (average 2.0 wt%), Al_2O_3 (average 2.9 wt%) and TiO_2 (average 0.09 wt%), similar to values for primitive mantle lherzolite. A plot of whole-rock CaO versus Al_2O_3 suggests that almost all of the Shuanggou samples have undergone ~25% partial melting with one sample showing 30% partial melting (Fig. 3a). A plot of whole-rock CaO versus X_{Mg} gives similar results (Fig. 3b). However, these can only be considered to be rough estimates because CaO can be easily mobilized during serpentinization and alteration.

Both the lherzolites and harzburgites contain spinel with similar Cr# [$100Cr/(Cr + Al)$] ranging from 30 to 56, indicating that these are I-type abyssal peridotites as classified by Dick and Bullen (1984), implying formation beneath a mid-oceanic ridge. Olivines and orthopyroxenes in the peridotites are highly magnesian (Fo of olivine = 90–91 and En of orthopyroxene = 90–92) (Zhang et al., 1992; Zhong, 1998).

5.2. Gabbro–diabase assemblage

Due to the paucity of fresh volcanic rock, the gabbro samples from the Shuanggou ophiolite are taken, at a first order

Table 1
Abundances of major oxides and trace elements of the Shuanggou ophiolite, SW China

Sample No.	HH-3	HH-4	HH-5	HH-32	HH-33	HH-34	HH-35	HH-18	HH-19	HH-20	HH-6	HH-7	HH-8
Rock types	U	U	U	U	U	U	U	D	D	D	G	G	G
Major oxides (wt%)													
SiO_2	39.25	39.35	39.10	38.61	37.19	39.13	38.30	48.34	49.67	47.67	37.61	36.86	36.56
TiO_2	0.06	0.09	0.08	0.02	0.01	0.10	0.09	0.97	1.71	1.05	0.72	0.74	0.66
Al_2O_3	1.98	3.52	2.42	2.08	0.98	1.94	3.54	15.44	13.35	14.92	11.72	12.63	12.93
Fe2O3t	7.58	7.87	8.22	8.43	8.14	8.51	7.84	9.52	12.73	9.63	9.32	9.96	11.66
MnO	0.08	0.12	0.11	0.08	0.13	0.11	0.12	0.15	0.14	0.16	0.19	0.17	0.18
MgO	37.11	34.97	35.82	35.77	36.72	34.46	34.53	8.60	6.52	8.98	18.72	16.05	11.50
CaO	0.78	2.02	1.26	0.11	1.44	2.06	1.71	11.82	9.88	11.31	13.35	16.64	20.63
Na_2O	0.00	0.00	0.00	0.00	0.00	0.00	0.00	2.14	3.24	2.44	0.01	0.00	0.00
K_2O	0.00	0.00	0.00	0.00	0.00	0.00	0.00	0.39	0.16	0.17	0.04	0.04	0.05
P_2O_5	0.02	0.02	0.02	0.02	0.02	0.02	0.02	0.10	0.17	0.10	0.03	0.04	0.04
LOI	12.53	11.44	12.80	14.16	15.08	13.50	13.50	2.32	1.97	2.95	7.66	6.75	5.72
Total	99.39	99.40	99.83	99.28	99.71	99.83	99.65	99.79	99.54	99.38	99.37	99.88	99.85
Trace elements (ppm)													
Th	0.01	0.01	0.01	0.00	0.00	0.01	0.00	0.06	0.15	0.06	0.02	0.02	0.01
Nb	0.07	0.07	0.05	0.04	0.04	0.11	0.05	0.90	1.93	0.94	0.46	0.25	0.24
Ta	0.08	0.06	0.04	0.01	0.01	0.02	0.01	0.07	0.15	0.07	0.06	0.05	0.05
Zr	2.72	2.89	4.53	0.33	1.17	3.18	3.84	57.30	115.00	60.70	37.80	36.20	23.60
Y	1.67	1.99	2.42	1.51	0.16	1.62	3.04	21.30	39.60	23.40	34.20	28.70	22.60
La	0.12	0.17	0.12	0.03	0.05	0.22	0.16	1.66	3.30	1.57	0.62	0.79	0.73
Ce	0.36	0.48	0.37	0.05	0.08	0.80	0.53	5.55	11.00	5.52	2.10	2.72	2.53
Pr	0.06	0.08	0.07	0.01	0.01	0.14	0.09	1.01	1.97	1.02	0.44	0.53	0.48
Nd	0.30	0.47	0.41	0.05	0.08	0.72	0.47	5.87	11.00	5.92	2.95	3.35	2.76
Sm	0.11	0.14	0.16	0.03	0.02	0.23	0.19	2.16	3.94	2.24	1.52	1.50	1.21
Eu	0.05	0.07	0.08	0.01	0.01	0.08	0.07	0.85	1.37	0.89	0.73	0.55	0.56
Gd	0.18	0.24	0.29	0.09	0.02	0.28	0.35	3.16	6.00	3.46	3.08	2.69	2.24
Tb	0.04	0.05	0.05	0.02	0.00	0.05	0.07	0.59	1.06	0.63	0.67	0.56	0.46
Dy	0.25	0.33	0.37	0.18	0.02	0.30	0.49	3.85	7.12	4.20	5.15	4.09	3.36
Ho	0.06	0.07	0.08	0.05	0.01	0.06	0.12	0.86	1.58	0.94	1.19	0.94	0.81
Er	0.17	0.20	0.25	0.16	0.02	0.18	0.36	2.48	4.58	2.64	3.42	2.86	2.32
Tm	0.03	0.03	0.04	0.03	0.00	0.03	0.06	0.37	0.68	0.40	0.50	0.42	0.34
Yb	0.20	0.22	0.25	0.19	0.03	0.19	0.37	2.34	4.23	2.54	2.86	2.56	2.03
Lu	0.04	0.03	0.04	0.03	0.01	0.03	0.05	0.35	0.65	0.39	0.39	0.36	0.29

Sample No.	HH-9	HH-10	HH-11	HH-12	HH-13	HH-14	HH-15	HH-16	HH-17	HH-21	HH-22	HH-31
Rock types	G	G	U	G	G	G	G	G	G	G	G	G
Major oxides (%)												
SiO_2	35.89	32.47	38.67	50.22	50.61	47.38	46.43	46.39	46.11	50.39	50.10	50.44
TiO_2	0.77	0.65	0.89	0.52	0.37	0.88	0.68	0.74	0.58	0.54	0.43	0.36
Al_2O_3	12.83	14.96	13.76	15.60	13.89	16.52	18.69	18.42	20.00	16.01	13.08	17.65
FeOt	10.93	13.78	15.10	8.16	6.16	9.01	8.05	8.16	6.43	6.82	6.42	6.52
MnO	0.16	0.16	0.21	0.12	0.10	0.15	0.14	0.13	0.11	0.11	0.11	0.10
MgO	14.96	15.43	12.02	7.62	9.95	8.29	7.88	7.74	6.91	7.55	10.45	7.03
CaO	17.42	14.28	13.53	11.47	13.53	11.29	11.61	10.86	11.83	12.82	14.17	11.12
Na_2O	0.00	0.00	0.04	3.11	2.34	2.48	2.28	2.38	2.75	2.70	2.09	3.46
K_2O	0.05	0.05	0.05	0.33	0.26	0.42	0.51	0.66	0.34	0.27	0.20	0.19
P_2O_5	0.04	0.03	0.04	0.05	0.04	0.09	0.07	0.08	0.07	0.08	0.05	0.07
LOI	6.68	8.07	5.64	2.13	2.00	2.94	2.98	3.77	4.52	2.29	2.36	2.39
Total	99.73	99.88	99.95	99.33	99.25	99.45	99.32	99.33	99.65	99.58	99.46	99.33
Trace elements (ppm)												
Th	0.02	0.00	0.00	0.05	0.06	0.06	0.04	0.05	0.03	0.04	0.06	0.48
Nb	0.36	0.23	0.03	0.56	0.37	0.88	0.60	0.61	0.47	0.42	0.51	1.10
Ta	0.05	0.05	0.03	0.06	0.04	0.07	0.05	0.06	0.04	0.04	0.05	0.11
Zr	39.90	38.90	31.90	37.30	32.70	50.70	37.90	43.70	30.80	31.60	62.80	81.70
Y	32.60	42.80	25.80	21.90	17.30	19.40	16.10	17.50	13.60	18.20	26.50	32.80
La	0.96	0.56	0.54	1.44	1.44	1.52	1.20	1.23	0.94	1.41	1.59	7.37
Ce	3.18	1.87	2.34	5.27	5.00	5.11	3.88	4.10	3.14	4.85	6.24	20.80
Pr	0.63	0.36	0.53	1.00	0.88	0.93	0.70	0.75	0.58	0.91	1.22	3.05
Nd	3.72	2.39	3.53	5.74	4.77	5.21	3.95	4.36	3.31	5.15	6.81	14.20
Sm	1.65	1.31	1.66	2.11	1.68	1.98	1.50	1.68	1.25	1.79	2.57	3.78

(*continued on next page*)

Table 1 (*continued*)

Sample No.	HH-9	HH-10	HH-11	HH-12	HH-13	HH-14	HH-15	HH-16	HH-17	HH-21	HH-22	HH-31
Rock types	G	G	U	G	G	G	G	G	G	G	G	G
Eu	0.69	0.64	1.30	0.96	0.61	0.81	0.71	0.73	0.57	0.89	0.74	1.05
Gd	3.07	3.06	3.07	3.21	2.50	2.88	2.30	2.53	1.95	2.69	3.66	5.04
Tb	0.67	0.73	0.63	0.59	0.46	0.53	0.42	0.47	0.36	0.48	0.71	0.87
Dy	5.10	6.14	4.65	3.91	3.06	3.52	2.87	3.10	2.44	3.20	4.70	5.58
Ho	1.22	1.66	1.08	0.88	0.69	0.78	0.64	0.72	0.54	0.71	1.03	1.25
Er	3.59	5.24	3.02	2.58	1.97	2.24	1.90	2.04	1.59	2.12	3.04	3.65
Tm	0.54	0.83	0.42	0.37	0.31	0.34	0.28	0.31	0.23	0.30	0.45	0.57
Yb	3.28	5.22	2.43	2.38	1.91	2.16	1.86	1.99	1.50	1.98	2.82	3.56
Lu	0.46	0.75	0.32	0.35	0.28	0.31	0.29	0.29	0.23	0.30	0.41	0.51

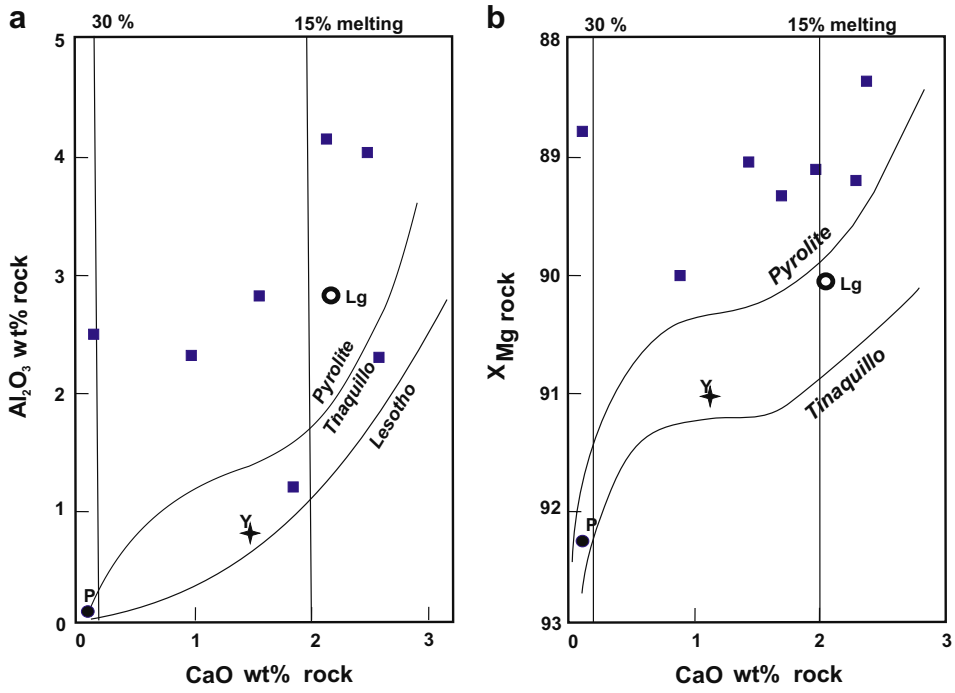

Fig. 3. (a) CaO versus Al_2O_3 diagram showing that most peridotites in the Shuanggou ophiolite have undergone ~25% partial melting. One sample may have undergone as much as 30% partial melting. The curves represent the trends of the refractory residues of pyrolite, Tinaquillo lherzolite and Lesotho lherzolite (Mysen and Kushiro, 1977). (b) The same result is seen in a whole-rock CaO versus X_{Mg} partial melting diagram. Lg (Liguria), Y (Yakuno) and P (Papua) ophiolites are plotted for comparison showing approximate degrees of partial melting (after Ishiwatari, 1985).

of approximation, to represent melt compositions. This approach is permissible because none of the samples have cumulate textures. Plots of the gabbro and diabase samples in Harker-type diagrams, with MgO as the fractionation index, show two populations that cannot be related by simple fractionation (Fig. 4). These two groups are best defined in plots of TiO_2, Fe_2O_3 and MnO. The other oxides show variable trends, particularly for CaO, Na_2O and K_2O, which are sensitive to alteration. In a Cr versus Y diagram (Pearce, 1982) the gabbros and diabases plot mostly in the MORB and volcanic arc basalt (VAB) fields (Fig. 5a). The Th/Yb versus Ta/Yb diagram shows that the majority of the samples plot within the MORB–WPB array (Fig. 5b).

To determine whether or not the whole-rock REE in the diabases and gabbros have been remobilized, the REE were plotted against three alteration-resistant incompatible elements, Y, Ti and Zr (Fig. 6). In general, the total REE increase smoothly with increases in these three elements indicating that the gabbros preserve their magmatic REE signatures, although the samples again fall into two distinct groups. In primitive mantle-normalized diagrams (Sun and McDonough, 1989) all samples, including the meta-peridotites, show negative Th and Nb anomalies. The meta-peridotites show pronounced negative Sr anomalies, whereas the gabbros exhibit both negative and positive Sr anomalies (Fig. 7). Compared to the primitive mantle, the meta-peridotites are depleted in all the trace elements that are incompatible during partial melting. Chondrite-normalized REE patterns for both the diabase and gabbro samples are indistinguishable from MORB patterns, except for one sample that exhibits LREE enrichment (Fig. 8a and b). Some samples also exhibit small positive or negative Eu

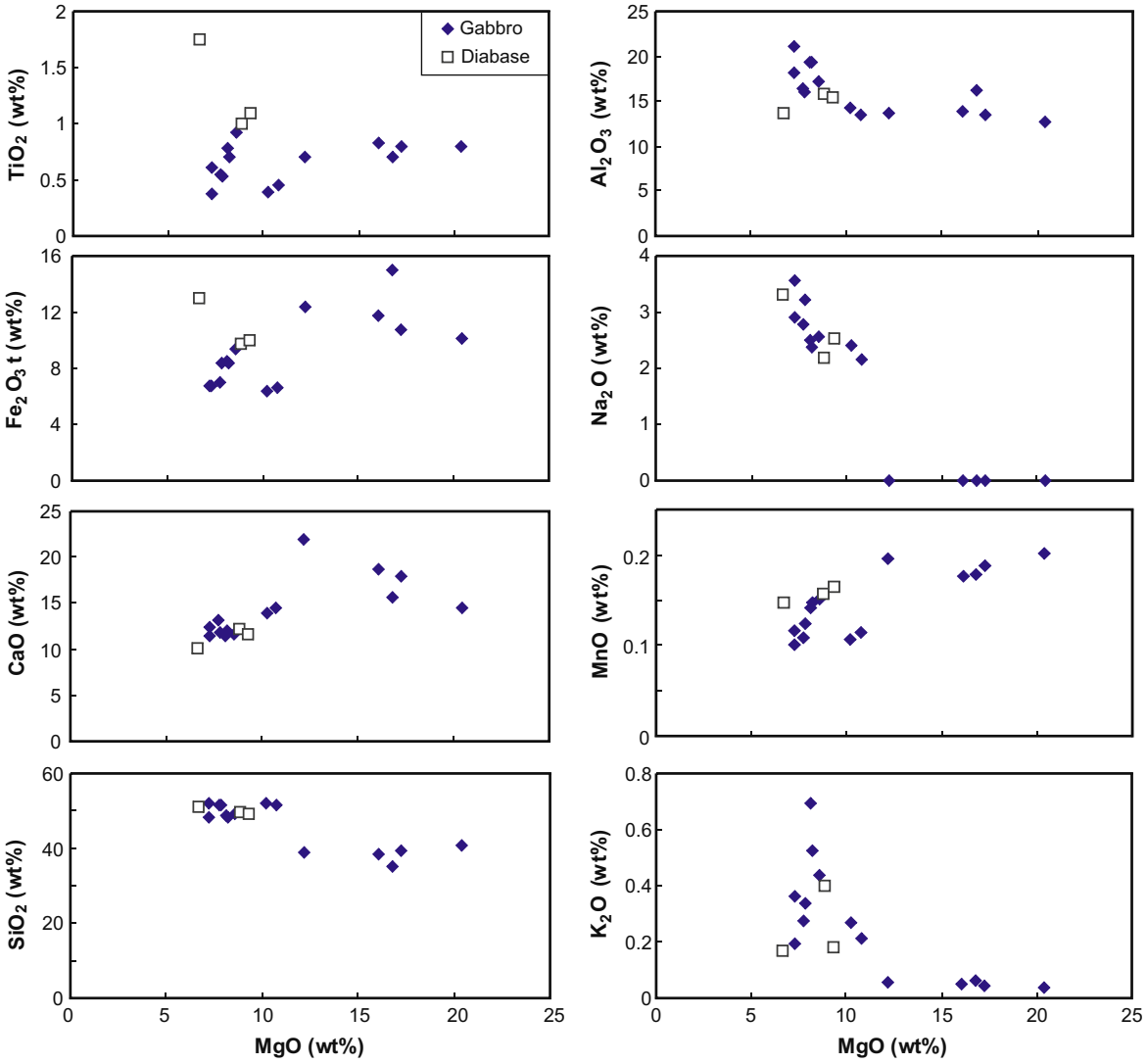

Fig. 4. Harker-type diagrams with MgO as the fractionation index. The two distinct groups can be recognized in most diagrams and they cannot be related by simple fractionation.

anomalies. Chondrite-normalized REE diagrams for the meta-peridotite exhibit relatively flat REE patterns with slight LREE depletion (Fig. 8a).

6. Discussion

6.1. Tectonic setting of the Shuanggou ophiolite

The meta-peridotite in the Shuanggou ophiolite is predominantly lherzolite with lesser amounts of harzburgite. A thin crustal section composed of gabbro, diabase and basalt directly overlies the meta-peridotite. There are no sheeted dikes or layered cumulate mafic and ultramafic rocks in the sequence. Ferruginous sediments overlie the ophiolite and, in some instances, lie directly on the meta-peridotite. All of these features are consistent with a low magmatic budget, which is characteristic of slow-spreading ridges (e.g., Dilek et al., 1998; Yumul, 2003). Extension and spreading in such settings is dominated by a magmatic processes mostly associated with listric faulting (e.g., Schaltegger et al., 2002). Radiolarian cherts are common in the early Carboniferous strata on top of the ophiolite, and the radiolarian assemblage belongs to a bathyal facies (Shen et al., 2001). The crystallization of plagioclase before pyroxene, as observed in the cumulate gabbro, is similar to the crystallization sequence observed in MORB (e.g., Dilek and Flower, 2003). The whole-rock geochemistry of the gabbros and diabases mimic that of MORB, although all samples have negative Th and Nb anomalies, suggesting a limited subduction influence. The spinel in the meta-peridotite has Cr# ranging from 30 to 56, suggesting approximately 12–18% partial melting for the peridotite (e.g., Hellebrand et al., 2001; Brunelli et al., 2003). The generally low degrees of partial melting in the meta-peridotite are consistent with the predominance of lherzolite and the slow-spreading character of the oceanic basin (Yumul, 2003) (Fig. 3a and b). The low degrees of partial melting noted in the Shuanggou ophiolite are similar to those

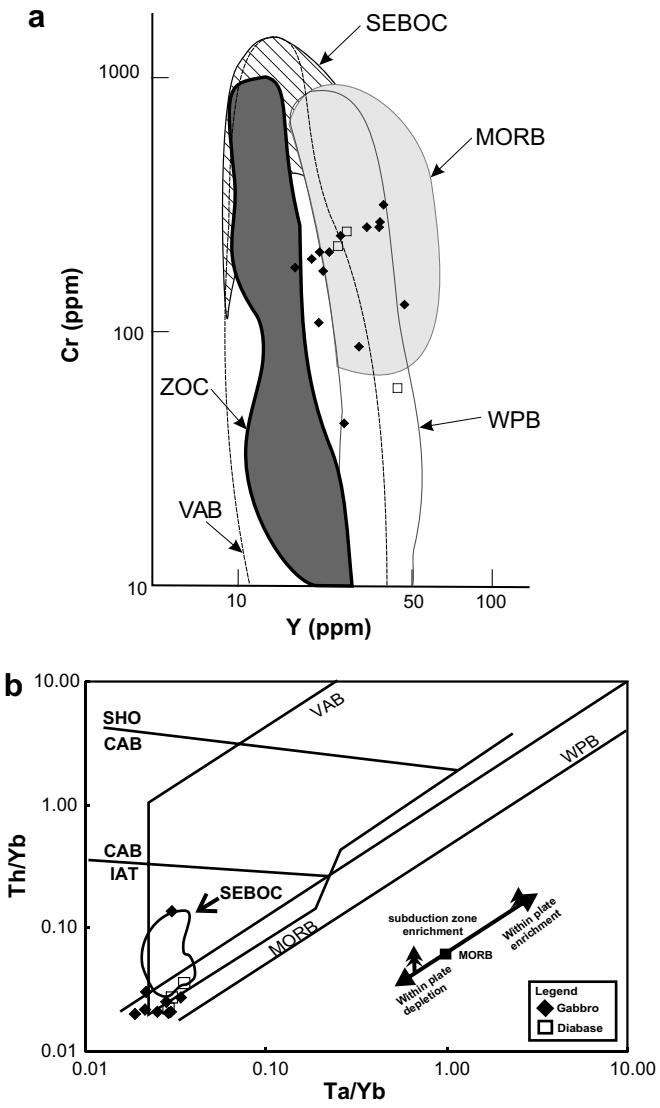

Fig. 5. (a) Cr versus Y diagram (after Pearce, 1982) showing that the gabbros and diabases of the Shuanggou ophiolite mostly plot in the mid-ocean ridge basalt (MORB) and volcanic arc basalt (VAB) fields (Wilson, 1994). Symbols: filled diamond, gabbro; open square, diabase. Fields for the Southeast Bohol Ophiolite Complex (SEBOC) and Zambales Ophiolite Complex (ZOC) fields are shown for comparison (after Yumul and Balce, 1994; Yumul et al., 2001). (b) Th/Yb versus Ta/Yb diagram showing that the majority of the samples plot within the MORB-WPB array (Wilson, 1994). The SEBOC field is shown for comparison (Faustino et al., 1998).

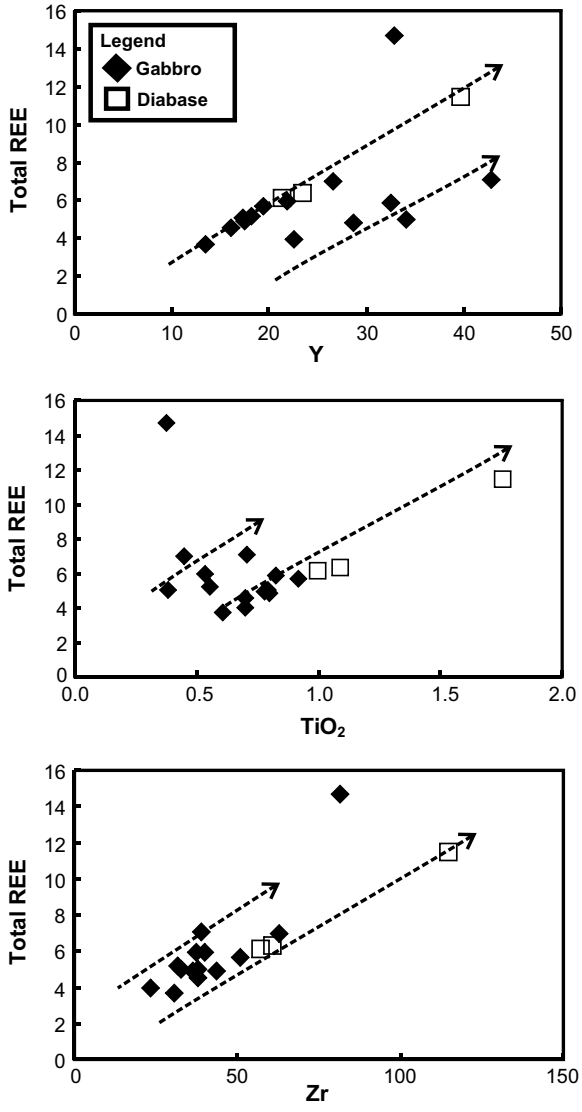

Fig. 6. Plot of total REE versus Y, TiO_2 and Zr. The coherent increase of the REE with increasing incompatible elements suggests that the REE were not remobilized during alteration.

observed in other Ailao Shan ophiolites (Wei et al., 1999). The presence of plagioclase in the peridotite is consistent with a low pressure (~5 kbar) regime. In summary, the available field and geochemical data suggest that the Shuanggou ophiolite was formed in a small, slow-spreading oceanic basin. The negative Th and Nb anomalies and tectonic discrimination diagrams suggest a limited subduction zone influence, perhaps indicating formation in a back-arc basin. Alternatively, these geochemical characteristics could be an inherited mantle feature (e.g., Moores et al., 2000).

6.2. Age of the Shuanggou ophiolite and its tectonic significance

Zhong (1998) reported an $^{40}Ar/^{39}Ar$ plateau age of 339 ± 14 Ma for clinopyroxene from a gabbro in the Shuanggou ophiolite. Jian et al. (1998a,b) obtained a SHRIMP zircon U–Pb age of 362 ± 41 Ma, which is similar to the $^{40}Ar/^{39}Ar$ age, although with a large uncertainty. An early Carboniferous age was determined for the radiolarian chert capping the ophiolite (Shen et al., 2001). The Shuanggou ophiolite meta-peridotite is overlain by the upper Triassic Yiwanshui Formation and some pebbles of meta-peridotite are included in the basal conglomerate of the Yiwanshui Formation (Zhang et al., 1992). From this relationship, it can be inferred that the ophiolite was emplaced prior to the late Triassic. Toward the southeast, in the Song Ma suture zone, the existence of a regional upper Carbonifer-

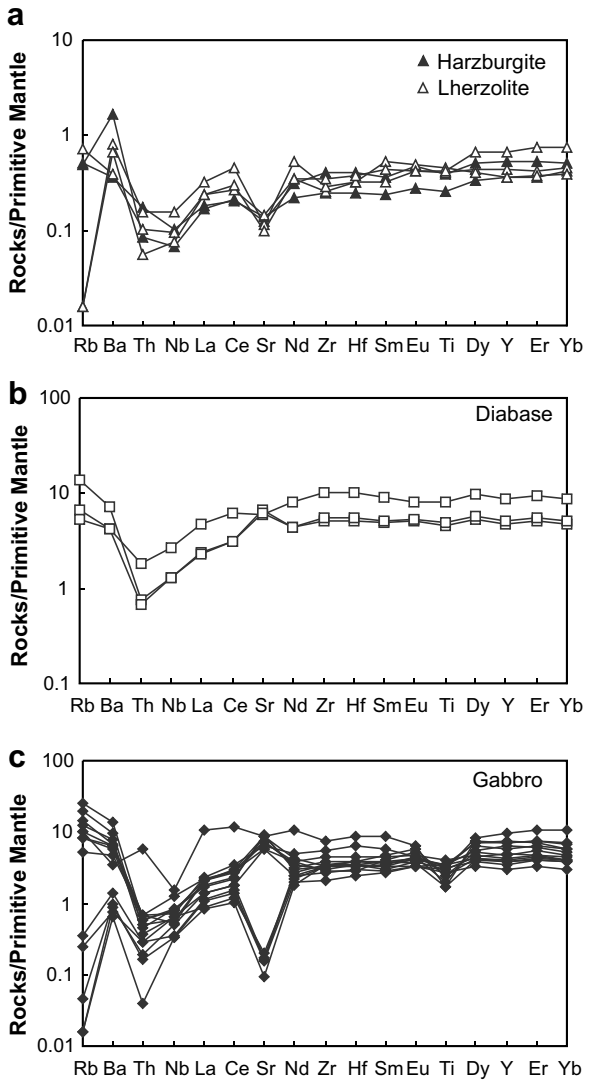

Fig. 7. Primordial mantle-normalized trace element patterns for (a) ultramafic rocks, (b) diabases and (c) gabbros. The primordial mantle data are from Sun and McDonough (1989). See text for discussion.

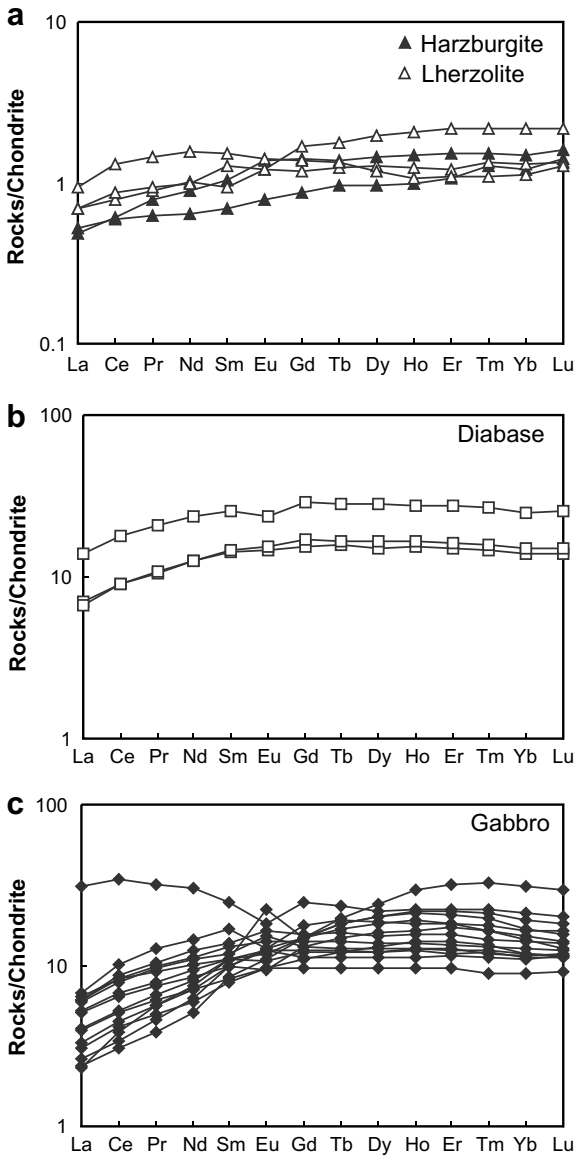

Fig. 8. Chondrite-normalized REE patterns for (a) ultramafic rocks, (b) diabases and (c) gabbros. Chondrite data are from Sun and McDonough (1989). See text for discussion.

ous unconformity (Deprat, 1914) may suggest an upper Paleozoic collision of the active margin of the Indochina Block with the South China Block (e.g., Fontaine and Workman, 1978; Leloup et al., 1995). Paleogeographic reconstruction implies a SW-directed subduction (based on present geographic setting) possibly in the mid-Paleozoic. The upper Paleozoic collision would reflect closure of the ocean basin between the two blocks. Emplacement of the Ailao Shan ophiolitic belt, of which the Shuanggou ophiolite is a part, occurred during this collision.

During Carboniferous and Permian time, the southwestern part of the South China Block was a passive margin in Paleo-Tethys, characterized by deposition of a thick sequence of continental clastic sedimentary rocks and continental flood basalts (Xiao et al., 2003). From east to west, Paleo-Tethyan lithosphere is represented by the Ailao Shan ophiolite in Yunnan, the Jinshajiang ophiolite in the central segment and the Kokoxili ophiolite in North Tibet. The existence of Paleo-Tethys between the Indochina and South China Blocks is supported by paleomagnetic data (Huang et al., 1992), which suggest that the ocean existed for over 100 Ma. The Ailao Shan oceanic lithosphere was subducted southward beneath the Indochina Block where a former active volcanic margin has been identified (Fontaine and Workman, 1978). At the same time, these two blocks drifted northward until they collided with the South China Block. Although the timing of collision of Indochina with South China is uncertain, emplacement of the Ailao Shan ophiolite must have occurred before Late Triassic because molasse deposits of that age unconformably overlie the ophiolite. In addition, post-collisional igneous assemblages have been dated at around 210–240 Ma (Yan et al., 2006). The amalgamation of these two blocks during the Triassic, as marked by the emplacement of the

Ailao Shan ophiolite, was associated with the opening of the Neo-Tethyan Ocean to the south.

7. Conclusions

The Shuanggou ophiolite formed in a small, slow-spreading oceanic basin. The emplacement of the ophiolite in the Ailao Shan orogenic belt marked the closure of the oceanic basin between the Indochina and South China Blocks.

Acknowledgements

Portions of this paper were written while G.P.Y. was in residence at Kumamoto University under a JSPS Visiting Scientist Fellowship. This study was also supported by a research grant from Chinese Academy of Sciences (to M.F.Z.). Mr. Tomas Tam III is thanked for help in preparing the figures. The authors wish to thank Prof. Paul T. Robinson and Prof. Yildirim Dilek for thorough reviews that helped to improve this paper.

References

Brunelli, D., Cipriani, A., Peyve, A., Bonatti, E., 2003. Mantle peridotites from the Bouvet Triple Junction Region, South Atlantic. Terra Nova 15, 194–203.

Chen, B.W., Xie, G.L., 1994. Evolution of the Tethys in Yunnan and Tibet. Journal of Southeast Asian Earth Sciences 9, 349–354.

Deprat, J., 1914. Etude des plissements et des zones d'ecrasement de la moyenne et basse riviere noire. Memoires du Service Geologique de l'Indochine 3, 1059.

Dick, H.J.B., Bullen, T., 1984. Chromian spinel as a petrogenetic indicator in abyssal and alpine-type peridotites and spatially associated lavas. Contributions to Mineralogy and Petrology 86, 54–76.

Dilek, Y., Moores, E.M., Furnes, H., 1998. Structure of modern oceanic crust and ophiolites and implications for faulting and magmatism at oceanic spreading centers. In: Buck, R., Karson, J., Delaney, P., Lagabrielle, Y. (Eds.), Faulting and Magmatism at Mid-Ocean Ridges. American Geophysical Union Monograph 106, pp. 219–266.

Dilek, Y., Flower, M.F.J., 2003. Arc-trench rollback and forearc accretion: 2. A model template for ophiolites in Albania, Cyprus, and Oman. In: Dilek, Y., Robinson, P.T. (Eds.), Ophiolites in Earth History, vol. 218. Geological Society London Special Publication, pp. 43–68.

Dong, Y.B., Zhu, B.Q., Chang, X.Y., Deng, S.X., 2000. Geochemistry of the two-type volcanic rocks from Ailaoshan suture zone and their tectonic implication. Geochemica 29, 6–13.

Faustino, D.V., Yumul Jr., G.P., Dimalanta, C., De Jesus, J., Barretto, J.L., 1998. Volcanic rocks of the Southeast Bohol Ophiolite Complex: a record of tectonic polarity reversal. AGU – Western Pacific Geophysics Meeting Abstract, Taipei, Taiwan, vol. 79, No. 24, p. W109.

Fontaine, H., Workman, D.R., 1978. Review of the geology and mineral resources of Kampuchea, Laos and Vietnam. In: Nutalaya, P. (Ed.), Geology and Mineral Resources of Southeast Asia. Asian Institute of Technology, Bangkok, pp. 538–603.

Hellebrand, E., Snow, E.J., Dick, H.J.B., Hoffmann, A.W., 2001. Coupled major and trace-element melting indicators in mid-ocean ridge peridotites. Nature 410, 677–681.

Hsu, K.J., Pan, G.T., Sengor, A.M., 1995. Tectonic evolution of the Tibetan Plateau: a working hypothesis based on the archipelago model of orogenesis. International Geology Review 37, 473–508.

Huang, K.N., Opdyke, N.D., Peng, X.J., Li, J.G., 1992. Paleomagnetic results from the Upper Permian of the eastern Qiangtang Terrane of Tibet and their tectonic implications. Earth and Planetary Science Letters 111, 1–10.

Hutchinson, C.S., 1975. Ophiolites in Southeast Asia. Geological Society of American Bulletin 86, 797–806.

Hutchinson, C.S., 1989. Geological Evolution of SE Asia. Oxford Monographs on Geology and Geophysics, vol. 13. Clarendon Press, Oxford, 368pp.

Ishiwatari, A., 1985. Igneous petrogenesis of the Yakuno ophiolite (Japan) in the context of the diversity of ophiolites. Contributions to Mineralogy and Petrology 89, 155–167.

Jian, P., Wang, X.F., He, L.Q., Wang, C.S., 1998a. U–Pb zircon dating of the Shuanggou ophiolite from Xinping County, Yunnan Province. Acta Petrologica Sinica 14, 207–212.

Jian, P., Wang, X.F., He, L.Q., Wang, C.S., 1998b. Geochronology of ophiolitic rocks from the Ailaoshan suture, Yunnan Province, south-western China, implications on palaeotethyan evolution. Geology and Mineral Resources of South China 1, 1–11.

Leloup, H.P., Arnaud, N., Lacassin, R., Kienast, J.R., Harrison, T.M., Trinh, P.T., Replumaz, A., Tapponnier, P., 2001. New constraints on the structure, thermochronology and timing of the Ailao Shan–Red River shear zone, SE China. Journal of Geophysical Research 106, 6683–6732.

Leloup, P.H., Harrison, T.M., Ryerson, F.J., Chen, W., Li, Q., Tapponnier, P., Lacassin, R., 1993. Structural, petrological and thermal evolution of a Tertiary ductile strike-slip shear zone, Diancang Shan, Yunnan. Journal of Geophysical Research 98, 6715–6743.

Leloup, P.H., Lacassin, R., Tapponnier, P., Scharer, U., Zhang, D.L., Liu, X.H., Zhang, L.S., Ji, S.C., Pan, T.T., 1995. The Ailao Shan–Red River shear zone (Yunnan, China), Tertiary transform boundary of Indochina. Tectonophysics 251, 3–84.

Li, X.Z., Liu, Z.Q., Pan, G.T., 1991. The dividing and evolution of tectonic units of Sanjiang, southwest China. Bulletin of the Chengdu Institute of Geology and Mineral Resources, Chinese Academy of Geological Sciences 13, 1–19.

Mercier, J.C., Nicolas, A., 1975. Textures and fabrics of upper mantle peridotites as illustrated by basalt xenoliths. Journal of Petrology 16, 454–487.

Metcalfe, I., 1996. Pre-Cretaceous evolution of SE Asian terranes. In: Hall, R., Blundell, D. (Eds.), Tectonic Evolution of Southeast Asia, 106. Geological Society London Special Publication, pp. 97–122.

Mo, X.X., Lu, F.X., Shen, S.Y., 1993. Tethyan Volcanism and Mineralization in Sanjiang Area. Geological Publishing House, Beijing, 267 p.

Moores, E.M., Kellogg, L.H., Dilek, Y., 2000. Tethyan ophiolites, mantle convection, and tectonic "historical contingency": a resolution of the "ophiolite conundrum". In: Dilek, Y., Moores, E.M., Elthon, D., Nicolas, A. (Eds.) Ophiolites and Oceanic Crust: New Insights from Field Studies and the Ocean Drilling Program. Geological Society of America Special Paper 349, pp. 3–12.

Mysen, B.O., Kushiro, I., 1977. Compositional variations of coexisting phases with degrees of melting of peridotites in the upper mantle. American Mineralogist 62, 843–865.

Pan, G.T., Chen, Z.L., Li, X.Z., 1997. The Formation and Evolution of Tectonics in the Eastern Tethys. Geological Publishing House, Beijing, pp. 1–218 (in Chinese).

Pearce, J.A., 1982. Trace element characteristics of lavas from destructive plate boundaries. In: Thorpe, R.S. (Ed.), Andesites. John Wiley and Sons, p. 548.

Qi, L., Hu, J., Gregoire, D.C., 2000. Determination of trace elements in granites by inductively coupled plasma mass spectrometry. Talanta 51, 507–513.

Schaltegger, U., Desmurs, L., Manatschal, G., Muntener, O., Meier, M., Frank, M., Bernoulli, D., 2002. The transition from rifting to sea-floor spreading within a magma-poor rifted margin: field evidence and isotopic constraints. Terra Nova 14, 156–162.

Sengor, A.M.C., 1984. The Cimmeride orogenic system and the tectonics of Eurasia. Geological Society of America Special Paper 195, 82p.

Sengor, A.M.C., 1987. Tectonic subdivisions and evolution of Asia. Bulletin of Technology University 40, 355–435.

Shen, S.Y., Wei, Q.R., Cheng, H.L., Mo, X.X., 2001. Characteristics and geotectonic implications of two sorts of silicalites in the Ailao Mountain belt, "Three-River" area. Acta Petrologica et Mineralogica 20, 42–46.

Sun, S.S., McDonough, W.F., 1989. Chemical and isotopic systematics of oceanic basalts: implications for mantle composition and process. In: Saunders, A.D., Norry, M.J. (Eds.), Magmatism in the Ocean Basins, vol. 42. Geological Society London Special Publication, pp. 313–345.

Sun, X.M., Zhang, B.L., Nie, Z.T., 1997. Formation and environment of ophiolites and ophiolitic mélange in the Jinshajiang belt, northwestern Yunnan. Geological Review 43, 113–120.

Tapponnier, P., Lacassin, R., Leloup, P.H., Schaerer, U., Zhong, D.L., Wu, H.W., Liu, X.H., Ji, S.C., Zhang, L.S., Zhong, J.Y., 1990. The Ailao Shan/Red River metamorphic belt: tertiary left-lateral shear between Indochina and South China. Nature 343, 431–437.

Wei, Q.R., Shen, S.Y., Yu, H.Z., 1999. The genesis of pyroxene basalts and plagioclase basalts in the Ailaoshan ophiolite zone, Yunnan. Tethyan Geology 23, 39–45.

Wilson, M., 1994. Igneous Petrogenesis – A Global Tectonic Approach. Chapman and Hall, London, 466 p.

Xiao, L., Xu, Y.G., Chung, S.L., He, B., Mei, H.J., 2003. Chemostratigraphic correlation of upper Permian lavas from Yunnan province, China: extent of the Emeishan large igneous province. International Geology Review 45, 753–766.

Yan, D.Y., Zhou, M.F., Wang, C.Y., Xia, B., 2006. Structural and geochronological constraints on the tectonic evolution of the Dulong-Song Chay tectonic dome in Yunnan Province, SW China. Journal of Asian Earth Sciences 28, 332–353.

Yumul Jr., G.P., 2003. The Cretaceous Southeast Bohol Ophiolite Complex, Central Philippines: evidence for formation in a fast spreading center. Journal of Asian Earth Sciences 21, 957–965.

Yumul Jr., G.P., Balce, G.R., 1994. Supra-subduction zone ophiolites as favorable hosts for chromitite, platinum and massive sulfide deposits. Journal of Southeast Asian Earth Sciences 10, 65–79.

Yumul Jr., G.P., Zhou, M.F., Tamayo, R.A., Maury, R.C., Faustino, D.V., Olaguera, F.O., Cotten, J., 2001. Onramping of cold oceanic lithosphere in a forearc setting: the Southeast Bohol Ophiolite Complex, Central Philippines. International Geology Review 43, 850–866.

Yunnan (Anonymous), 1990. Regional geology of Yunnan Province. Geological Memoires Series, vol. 21. Geological Press, Beijing (in Chinese).

Zhang, Q., Zhang, K.W., Li, D.Z., 1992. Mafic–Ultramafic Rocks in the Hengduan Mountains Region. Science Press, Beijing.

Zhong, D.L., 1998. Paleo-Tethyan Orogenic Belt in the Western Yunnan and Sichuan Province. Science Press, Beijing, pp. 1–231.